Human coronaviruses disassemble processing bodies

Carolyn-Ann Robinson[1*], Mariel Kleer[1*], Rory P. Mulloy[1,2*], Elizabeth L. Castle[3], Bre Q. Boudreau[4] and Jennifer A. Corcoran[1,4 #]

[1]Microbiology, Immunology and Infectious Diseases Department and Charbonneau Cancer Research Institute, University of Calgary, Calgary, AB, Canada.
[2]Department of Biochemistry, Microbiology and Immunology, University of Ottawa, Ottawa, ON, Canada.
[3] School of Biomedical Engineering, University of British Columbia, Vancouver, BC, Canada.
[4]Department of Microbiology and Immunology, Dalhousie University, Halifax, NS, Canada.
[*]Equal contribution
[#]Corresponding Author

Abstract

The *Coronaviridae* are a family of viruses with large RNA genomes. Seven coronaviruses (CoVs) have been shown to infect humans, including the recently emerged severe acute respiratory syndrome coronavirus 2 (SARS-CoV-2), the cause of coronavirus disease of 2019 (COVID-19). The host response to CoV infection is complex and regulated, in part, by intracellular antiviral signaling pathways triggered in the first cells that are infected. Emerging evidence suggests that CoVs hijack these antiviral responses to reshape the production of interferons and proinflammatory cytokines. Processing bodies (PBs) are membraneless ribonucleoprotein granules that mediate decay or translational suppression of cellular mRNAs; this is particularly relevant for proinflammatory cytokine mRNA which normally reside in PBs and are repressed. Emerging evidence also suggests that PBs or their components play important direct-acting antiviral roles, providing a compelling reason for their frequent disassembly by many viruses. No information is known about how human CoVs impact PBs. Here, we provide data to show that infection with the human CoV, OC43, causes PB disassembly. Moreover, we show that several SARS-CoV-2 gene products also mediate PB loss and virus-induced PB loss correlates with elevated levels of proinflammatory cytokine mRNAs that would normally be repressed in PBs. Finally, we demonstrate that stimulating PB formation prior to OC43 infection restricts viral replication. These data suggest that SARS-CoV-2 and other CoVs disassemble PBs during infection to support viral replication and evade innate immune responses. As an unintended side effect, the disassembly of PBs enhances translation of proinflammatory cytokine mRNAs which normally reside in PBs, thereby reshaping the subsequent immune response.

24

25 **Introduction**

26 PBs are ubiquitous, biomolecular condensates that form via liquid-liquid phase separation of
27 proteins with regions of intrinsic disorder, and from RNA-protein and RNA-RNA interactions
28 (1-5). PBs are comprised of the enzymes required for mRNA turnover, including those needed
29 for decapping (Dcp2 and co-factors Dcp1a and Edc4/Hedls) and decay of the RNA body (5'-3'
30 exonuclease Xrn1 and RNA helicase Rck/DDX6) and some components of the RNA-induced
31 silencing complex (2,6). The RNA found in PBs consists of one third of all coding transcripts
32 which are poorly translated and non-coding RNAs (2,4,7,8). mRNA transcripts, consisting
33 predominantly of grouped regulatory mRNAs with related biological functions, are delivered to
34 PBs by RNA-binding proteins (RBPs) (2,4). One such group bear destabilizing AU-rich elements
35 (AREs) in their 3'-untranslated regions (3'-UTRs) and encode potent regulatory molecules like
36 growth factors, pro-inflammatory cytokines, and angiogenic factors, making their turnover
37 and/or suppression in PBs fundamental to our physiology (9-11). We and others showed that the
38 presence of visible PBs correlates with increased turnover/suppression of ARE-mRNAs (11-15).
39 Conversely, when PBs are lost, constitutive ARE-mRNA suppression is reversed. This provides
40 cells with a means to rapidly respond to stimuli that disassemble PBs to produce
41 proinflammatory cytokines, making PB disassembly an important yet underappreciated
42 regulatory mechanism that tunes the production of potent proinflammatory cytokines that contain
43 AREs, molecules like IL-6, IL-8, IL-1β, and TNF (9).

44

45 PBs are constitutive, dynamic ribonucleoprotein (RNP) granules that change in size and number
46 in response to different stimuli. We and others have shown that stressors that activate the
47 p38/MK2 MAP kinase pathway, as well as many virus infections elicit PB disassembly
48 (12,13,15-18). Disassembly can occur by a direct interaction between a viral protein(s) and a PB
49 component that is subsequently re-localized to viral replication and transcription compartments
50 (vRTCs) (19-21) or cleaved by viral proteases (21-23). Viruses can also cause PB disassembly
51 indirectly by activating p38/MK2 signaling (12,13). Despite numerous reports of viral gene
52 products that trigger PB disassembly, corresponding reports of viral gene products that stimulate
53 PB formation are rare, which suggests that PBs possess direct antiviral function and their
54 disassembly may favour viral replication in ways that we fail to grasp (24). Even though other

55 RNPs such as stress granules have emerged as important components of our antiviral defenses
56 that contribute to sensing virus and triggering innate immune responses (25-27), the evidence to
57 support a direct antiviral role for PBs is less well established (24). A direct-acting antiviral role
58 has been defined for several PB-localized enzymes that impede viral replication (e.g.
59 APOBEC3G, MOV10). However, in these cases, the mechanism of viral restriction was
60 attributed to the enzymatic activity of the PB protein(s) and its localization to PBs was not
61 deemed as significant (20,21,23,28-35). PBs also harbour antiviral proteins that are important for
62 innate immune signaling, diverting them and keeping them ready for the inducement of the
63 desired antiviral response (20,36). It remains unclear if organization of particular proteins in PBs,
64 or the higher order condensation of many proteins into the PB, regulates its antiviral activities.
65 Nonetheless, the disassembly of PBs by diverse viruses strongly suggests their importance.
66
67 The family *Coronaviridae* includes seven viruses that infect humans, including the four
68 circulating 'common cold' coronaviruses (CoVs), HCoV-OC43, HCoV-229E, HCoV-NL63, and
69 HCoV-HKU1 and three zoonotic viruses that cause severe disease in humans: MERS-CoV,
70 SARS-CoV, and the recently emerged SARS-CoV-2 (37,38). The latter is the infectious cause of
71 coronavirus disease of 2019 (COVID-19). When severe, COVID is characterized by aberrant
72 proinflammatory cytokine production, endothelial cell (EC) dysfunction and multiple organ
73 involvement and has resulted in more than a million deaths worldwide thus far (39-44). Despite
74 previous CoV epidemics, we do not yet appreciate precisely how SARS-CoV-2 infection causes
75 the pathology observed in COVID and urgently need to define these molecular mechanisms to
76 inform novel therapeutic strategies. Although all CoVs encode multiple proteins that hijack
77 antiviral and interferon (IFN) responses (45), SARS-CoV-2 excels in this regard and a
78 mismanaged IFN response is emerging as a major clinical determinant of COVID outcomes (45-
79 48). In support of this, new evidence continues to reveal the multitude of mechanisms used by
80 SARS-CoV-2 to out compete antiviral responses (49-53). For example, four SARS-CoV-2 non-
81 structural proteins (nsp) were recently reported to each interact with specific cellular RNA
82 targets to dramatically diminish IFN-β production and promote viral propagation (52).
83
84 To contribute to an enhanced understanding of how SARS-CoV-2 and other CoVs usurp cellular
85 antiviral responses and alter cytokine mRNA expression profiles, we performed an analysis of

86 PBs. There is no published literature on human CoVs and PBs, and only two previous reports
87 mentioned PB dynamics after CoV infection. Murine hepatitis virus (MHV) was reported to
88 increase PBs at early infection times, while transmissible gastroenteritis coronavirus (TGEV)
89 infected cells displayed complete PB loss by 16 hours post infection (24,54-56). We now present
90 the first evidence to show that PBs are targeted for disassembly by a human CoV. We also show
91 that SARS-CoV-2 encodes multiple proteins that when expressed alone are capable of causing
92 PB loss, supporting a coordinated effort by CoVs to disassemble these granules. Finally, we
93 show that prior formation of PBs restricts infection with OC43, delaying the expression of the
94 viral nucleocapsid protein and preventing infectious progeny production. Taken together, these
95 results suggest PBs play central role in the cellular antiviral responses to CoV infection.
96
97

98 **Results**

99

100 A screen of SARS-CoV-2 genes reveals mediators of PB loss

101 The genome of SARS-CoV-2 is predicted to contain up to 14 open reading frames (ORFs). The
102 two N-terminal ORFs (1a and 1ab) encode two large polyproteins which are processed by viral
103 proteases into 16 non-structural proteins (nsp1-16) essential for viral genome replication and
104 transcription (37). The 3' end of the SARS-CoV-2 genome is predicted to code for ORFs that are
105 expressed from 9 subgenomic mRNAs (57). Among these are the four structural proteins spike
106 (S), envelope (E), membrane (M) and nucleocapsid (N) and up to 9 potential accessory proteins,
107 not all of which have been validated in infected cells (37). To test the role of SARS-CoV-2 gene
108 products in PB disassembly, we obtained a plasmid library of 27 SARS-CoV-2 genes from the
109 Krogan lab; this library included 14 nsps (excluding nsp3 and nsp16), all structural (S, E, M, N)
110 and candidate accessory genes (ORFs 3a, 3b, 6, 7a, 7b, 8, 9b, 9c, 10) and a catalytically inactive
111 mutant version of the nsp5 3C-like protease (C145A) (57). We individually transfected each
112 plasmid into HeLa cells that express a Dox-inducible GFP-tagged version of the PB-resident
113 protein, Dcp1a (6). When fixed, these GFP-positive puncta co-stain with endogenous PB
114 proteins such as the RNA helicase DDX6/Rck (Fig 1A) and the decapping co-factor hedls/Edc4
115 (Fig S1). While control cells or those transfected with the envelope (E) protein displayed DDX6-
116 positive PBs, PBs were largely absent after transfection of six SARS-CoV-2 genes including the
117 viral nucleocapsid (N) and the accessory gene, ORF7b (Fig 1A). We quantified number of
118 DDX6-positive PBs per cell for each transfection using CellProfiler, as in (58). This
119 quantification was performed in two different ways. In most cases, transfected cells were
120 identified by co-staining for the Strep-tag II fused to each gene, as shown for N, E and ORF7b
121 (Fig 1A). In such cases, we were able to count PBs only in cells with positive staining only and
122 not count PBs in bystander cells (Fig 1B, thresholded). These data identified two SARS-CoV-2
123 proteins that may cause PB loss in a cell autonomous manner: ORF7b and N (Fig 1B). For the
124 remaining transfections (nsp1, nsp5, nsp6, nsp11, nsp13, nsp14, ORF3b, ORF6, ORF9b, ORF9c)
125 immunostaining for the Strep-tag II was not robust and we were unable to threshold our PB
126 counts using CellProfiler. In these samples, we quantified PBs in all cells (Fig 1B,
127 unthresholded). These data identified four additional SARS-CoV-2 proteins that may cause PB
128 loss: ORF3b, nsp1, nsp6 and nsp11 (Fig 1B). We verified the expression of all constructs,

129 including low expressors (nsp1, nsp5, nsp6, nsp11, nsp13, nsp14, ORF3b, ORF6, ORF9b and
130 ORF9c) by immunoblotting whole cell lysates harvested from parallel transfections (Fig 1C). We
131 were unable to detect nsp4 and ORF10 by immunoblotting; however, we did visualize these
132 proteins in immunostained samples. Consistent with previous work (57), we were unable to
133 detect nsp6 by immunoblotting or by immunostaining, despite our observation that these cells
134 appear to have less DDX6-positive puncta than our controls (Fig 1B, C).
135
136 A screen of SARS-CoV-2 genes reveals enhancers of an ARE-containing luciferase reporter
137 We performed a secondary reporter screen to identify SARS-CoV-2 proteins that enhanced the
138 activity of a firefly luciferase (FLuc) reporter containing an ARE sequence in its 3' UTR,
139 rendering the mRNA sensitive to constitutive turnover or translational suppression in PBs (59).
140 For this reason, control samples display extremely low levels of FLuc luminescence relative to a
141 non-ARE renilla luciferase (RLuc) transfection control, that reflects the turnover or suppression
142 of the FLuc mRNA (Fig 2A). When reporter constructs are co-transfected with the positive
143 control protein, KapB, which we have previously shown to cause PB disassembly and elevate the
144 FLuc ARE-mRNA reporter (13,59), the relative luminescence is enhanced ~50-fold (Fig 2B).
145 After co-transfection with the SARS-CoV-2 gene library, we identified three SARS-CoV-2
146 proteins that significantly elevated relative luminescence as well as or better than KapB: nsp1
147 (150-fold), nsp14 (80-fold), and ORF7b (40-fold), and two others that elevated luminescence 10-
148 20-fold: nsp13 and ORF6 (Fig 2B). Of these ARE-mRNA regulating SARS-CoV-2 gene
149 products, two overlap with those we showed to cause PB loss, nsp1 and ORF7b (Fig 1).
150
151 Validation of SARS-CoV-2 genes that cause PB loss in primary endothelial cells
152 Endothelial cells (ECs) have emerged as playing a significant role in severe COVID, they are
153 also sources for many of the cytokines elevated in severe disease and are infected by SARS-
154 CoV-2 (48,60-63). We validated top hits from our PB and ARE-containing reporter screen in
155 human umbilical vein endothelial cells (HUVECs) that were transduced with recombinant
156 lentiviruses expressing N, nsp14 or a vector control. Transduced cells were selected and stained
157 for the endogenous PB marker protein DDX6 and for the Strep-tag II on each of SARS-CoV-2
158 constructs. Compared to the control, we observed PB loss in N-expressing cells and a decrease in
159 PB numbers in the nsp14-transduced cell population (Fig 3). We also observed that in some

160 cells, nsp14 staining, although usually difficult to detect, overlapped with DDX6-positive puncta
161 in nsp14-transfected HeLa cells (Fig 3B, C). The significance of this observation is unclear and
162 we are investigating it further.
163
164 Infection of endothelial cells with human coronavirus causes PB loss
165 To understand if PBs were lost during infection with human coronaviruses, we established an
166 infection model for the human CoV, OC43, in HUVECs. We tested the ability of OC43 to enter
167 and replicate in these primary cells and confirmed that HUVECs are permissive to OC43 (Fig
168 4A). We then performed a time-course experiment wherein OC43-infected HUVECs were fixed
169 at various times post infection and stained for DDX6 (PBs) and the viral nucleocapsid (N)
170 protein to denote infected cells. We observed that PBs were lost after infection with OC43 but
171 not lost over the time course of the experiment in our mock-infected control cells (Fig 4A-B).
172 These results showed that PB counts were significantly diminished at 12 and 24 hpi (Fig 4A-B).
173 To determine if the reduced PB counts correlated with changes to cytokine mRNA levels, we
174 harvested total RNA from OC43-infected cells at 24 hpi and performed RT-qPCR for two ARE-
175 containing cytokine transcripts, IL-6 and IL-8 (Fig 4C). Consistent with the observed reduction
176 in PBs, the steady-state levels of IL-6 and IL-8 mRNA both increased ~20-fold compared to
177 uninfected cells (Fig 4C). We also observed, in some infected cells, DDX6-positive puncta
178 reappeared at 24 hpi, but these puncta did not resemble PBs in terms of their size or shape but
179 were larger, non-spherical aggregates. It is unclear at this time if these DDX6-positive
180 aggregates represent vRTCs or stress granules, another RNP granule that viruses manipulate
181 (25,26). Further experiments will determine the nature of these aggregates.
182
183 PBs restrict coronavirus infection
184 Since SARS-CoV-2 encodes six proteins that induce PB loss and infection with OC43
185 recapitulates this loss, we hypothesized that PBs may be able to restrict coronavirus infection. To
186 test this, we used lentiviruses to deliver the fluorescently-labeled PB protein, GFP-Dcp1a, or a
187 control GFP protein to HUVECs prior to infecting with OC43. At various times post infection,
188 cells were fixed and stained for the viral nucleocapsid (N) protein (Fig 5A). Although OC43 was
189 able to express N in GFP-positive control cells, we observed viral N gene expression was
190 restricted in cells that expressed GFP-Dcp1a (Fig 5A). The restriction was most pronounced at

191 6hpi, when we observed only ~20% of GFP-Dcp1a-positive cells were visibly infected,
192 compared to the GFP-only controls (Fig 5B). At later infection times, more N gene expression
193 was observed in cells also expressing GFP-Dcp1a, suggesting that OC43 infection was able to
194 overcome the restriction imposed by GFP-Dcp1a (Fig 5B). Next, we examined if an increased
195 dose of the GFP-Dcp1a lentivirus, that should elicit the formation of more PBs, would increase
196 the restrictive phenotype (Fig 5C). HUVECs were transduced with 5-fold more GFP-Dcp1a
197 lentivirus than in Fig 5B, infected with OC43, and the infected cell supernatant was collected at
198 24hpi (Fig 5C). The amount of OC43 infectious particles produced in each condition was
199 determined using a TCID50 assay (64). Infectious OC43 particles were produced from control
200 cell populations transduced with the GFP virus and there was no significant difference in viral
201 particles produced after transduction with a lower dose of GFP-Dcp1a lentivirus (Fig 5C).
202 However, the addition of 5-fold more GFP-Dcp1a lentivirus prior to OC43 infection restricted
203 viral replication and no infectious OC43 particles were detected in the 24hpi-supernatant taken
204 from these cells (Fig 5C). Taken together, these data show that PB fortification prior to OC43
205 virus infection restricts virus replication, providing a compelling reason why SARS-CoV-2
206 would coordinate an attack on cellular PBs using multiple viral proteins.
207
208

209 **Discussion**

210 In this manuscript, we present data to show that the human CoV, OC43, causes PB loss during
211 infection. The loss of PBs correlates with elevated steady-state levels of two PB-regulated
212 cytokines, IL-6 and IL-8. Using a gene library, we also identify six candidate gene products
213 encoded by SARS-CoV-2 that are capable of inducing PB loss and three candidate gene products
214 that stabilize an ARE-containing luciferase reporter. Moreover, we present evidence that prior
215 fortification of PB granules using overexpression of the PB protein, GFP-Dcp1a, restricts the
216 infectious cycle of OC43, delaying viral nucleocapsid protein production and preventing
217 infectious progeny production. These data support our model that PBs are antiviral granules
218 designed to protect cells from viral invaders.

219

220 Multiple SARS-CoV-2 gene products highlight the diversity of approaches used by one virus to
221 induce PB loss

222 We screened 27 SARS-CoV-2 gene products by transfection in HeLa cells (57) and identified six
223 candidates that reduce PB numbers including the viral nucleocapsid protein (N), the viral host
224 shutoff factor (nsp1), non-structural proteins nsp6 and nsp11, and accessory proteins ORF7b and
225 ORF3b (Fig 1). The most significant of these candidates was the N protein, which we also
226 showed caused endogenous PB loss in primary ECs (Fig 3). N is a multifunctional RNA-binding
227 protein (RBP) that coats the viral genome and induces phase separation to promote viral particle
228 assembly (37,65-68). N possesses several non-specific RNA-binding regions and is
229 phosphorylated in its central serine-arginine (SR-rich) domain (68,69). SARS-CoV-2 N also
230 contains three putative NLS sequences (70). One possible reason for PB loss may be the
231 indiscriminate RNA binding of N protein which acts as sponge for RNA, pulling it out of
232 cytoplasm, reducing the RNA-protein interactions required for phase separation of PBs (3). We
233 are currently engaged in site-directed and truncation mutagenesis studies to determine the precise
234 region(s) of N that are essential for its effect on PBs (71). Another PB-regulating SARS-CoV-2
235 protein we discovered is the bifunctional enzyme, nsp14, which possesses an N-terminal
236 exonuclease domain (ExoN) required for proofreading of the CoV polymerase complex and a C-
237 terminal N-methyltransferase (MTase) domain that contributes to viral RNA capping (37,72).
238 Nsp14 caused PB loss in our EC validation studies yet it did not cause PB loss in HeLa cells (Fig
239 1, 3). Though we are unclear of the precise reason for these discrepant results, one consideration

240 is that GFP-Dcp1a expression in HeLa cells makes PBs more stable and their disassembly more
241 difficult. It was also quite difficult to detect the expression of nsp14 in HeLa cells after their
242 transfection, although nsp14 was detected by immunoblotting; therefore, PBs were counted in all
243 cells, and the results were not specific for cells that expressed nsp14 (Fig 1). In contrast, in our
244 EC validation studies we selected for transduced cells; thus, all ECs contain nsp14 even if the
245 staining is low (Fig 3). This may explain the significant PB loss observed in ECs and not in
246 HeLa cells. Finally, we observed that nsp14 occasionally formed small puncta that overlapped
247 with DDX6-positive PBs in both HeLa cells and ECs (Fig 3A, 3C). There are no previous reports
248 of any other CoV proteins co-localizing to PBs. The significance of this observation remains
249 unclear. We will continue to interrogate nsp14 localization using confocal microscopy and
250 immunoprecipitation assays. Nsp14 was also a significant hit in the luciferase reporter assay (Fig
251 2), suggesting that nsp14 promotes the stabilization or translation of PB-localized, ARE-
252 containing cytokine mRNA. Consistent with this, alphacoronavirus nsp14 enhanced TNF and
253 IFN-β (both these mRNAs contain AREs) independent of its enzymatic functions, a phenotype
254 that is consistent with a PB-regulating protein (73).
255
256 Our initial validation efforts have focused on nsp14 and N (Fig 3); however, our screens did
257 highlight other SARS-CoV-2 proteins that may regulate PBs to enhance translation of ARE-
258 mRNAs. These include the top hit in our luciferase screen, nsp1. All CoVs encode a host shutoff
259 protein called nsp1 that is the first protein expressed after virus entry and an important IFN
260 antagonist that limits IFN and interferon-stimulated gene translation (52,74). SARS-CoV-2 nsp1
261 binds to 18S rRNA and the blocks the mRNA entry channel in the 40S ribosomal subunit,
262 thereby blocking translation (52,75). Given its role in translation shutoff and RNA decay, we
263 were initially concerned that nsp1-mediated elevation in the ARE-containing FLuc reporter was
264 non-specific because we observed low levels of the RLuc control that could suggest global
265 translation shutoff (52,76-78). However, stress-responsive cellular transcripts are often resistant
266 to the action of nsp1and other viral shutoff proteins suggesting that the sequestration of
267 regulatory transcripts in PBs is a strategy used by cells to withstand viral host shutoff (74,77,79).
268 For this reason, PB-regulated transcripts like the ARE-containing FLuc reporter may be resistant
269 to nsp1-mediated shutoff (Fig 2). We are currently validating if nsp1 is a PB-regulating viral
270 protein in ECs and will explore its effects on cytokine mRNA levels. In addition, ORF7b and the

271 short ORF3b are intriguing hits because both are accessory proteins that have been reported to
272 either activate the kinase p38 (an inducer of PB disassembly) or antagonize IFN responses
273 (53,80). Not picked up in our screen, the viral 3C-like protease, nsp5, is also of particular interest
274 because porcine CoV nsp5 cleaves Dcp1a, an event that would be predicted to cause PB
275 disassembly (81). Although nsp6 and nsp11 were top hits in our unthresholded PB screen (Fig
276 1), their expression is either toxic or difficult to detect and we are engaged in developing
277 strategies to minimize these issues and study them further.
278
279 PBs are antiviral granules that restrict CoV infection
280 We used the human CoV, OC43, to infect ECs and show that virus infection caused significant
281 PB loss at 12 and 24 hpi (Fig 4). We then fortified PBs using the overexpression of GFP-Dcp1a
282 and showed that PB fortification before infection delayed the visual expression of viral
283 nucleoprotein and restricted the production of infectious viral particles (Fig 5). However, the
284 precise details of the mechanism of restriction remain unclear. We are engaged in ongoing time
285 course experiments to determine if the restrictive phenotype represents a delay of viral progeny
286 production or a complete block. It is also unclear if the prior GFP-Dcp1a overexpression restricts
287 OC43 replication due to a direct antiviral role of the Dcp1a enzyme itself or its ability to promote
288 the formation of larger PBs (82,83). GFP-Dcp1a overexpression is a common approach used to
289 visualize PBs, and we know these GFP-positive puncta co-stain with endogenous PB proteins
290 (Fig 1) (82). However, GFP-Dcp1a puncta are larger and may be more stable than endogenous
291 PBs (56,83). Our ongoing work will utilize other molecular tools that regulate PB dynamics to
292 determine if certain PB resident proteins exert antiviral properties independent from the
293 formation of the PB granule itself. We are currently engaged in experiments to overexpress
294 different PB proteins that have roles in RNA decay (Dcp1a, DDX6 RNA helicase, the decapping
295 cofactor hedls/Edc4 or the exonuclease Xrn1) as well as PB proteins that do not directly mediate
296 RNA decay but play an important condensation role for PB granule formation (Lsm14A, 4E-T)
297 (3,4,84). Each of the proposed proteins will affect PBs differently when overexpressed: Dcp1a,
298 hedls/Edc4 and DDX6 increase PB formation, with Dcp1a expression inducing larger granules
299 than the others, Dcp2 has no effect on granule size/number, and Xrn-1 eliminates PBs because it
300 increases mRNA decay (4,83-86). We predict that other GFP-tagged PB proteins that promote
301 molecular condensation of PBs, such as GFP-DDX6, will also restrict OC43 infection.

302 Conversely, we expect that the overexpression of Xrn1 will promote viral infection (as shown by
303 others (34)) because it prevents PB formation, even though it can degrade viral RNA.
304
305 There is increasing evidence in support of our hypothesis that the antiviral role of PB-localized
306 enzymes is promoted by phase separation of molecules into PBs and that the antiviral function of
307 these molecules is lost when PB granules decondense. This has been previously proposed for
308 decapping complexes, the enzymatic activity of which is increased by phase separation and
309 decreased in solution (3-5). However, for PB-localized enzymes that have established antiviral
310 effects, (e.g. APOBEC, MOV10), their ability to restrict virus infection has previously been
311 attributed to their enzymatic activity rather than their localization to PBs (20,21,23,29-35,82).
312 Therefore, it is not yet clear if the antiviral capability of PBs relies on their formation into
313 biomolecular condensates. Here, we consider that the antiviral restriction promoted by PB-
314 localized enzymes requires the granule formation for optimal function. By that definition, factors
315 that promote PB condensation may also be antiviral. Therefore, in part one of our model, we
316 propose that PBs are direct-acting antiviral granules that can restrict virus infection when present
317 as visible condensates; for this reason, they are targeted by disassembly by most viruses.
318
319 <u>PBs interact with other innate immune pathways to regulate antiviral signaling</u>
320 One possibility is that PBs are antiviral because their proteins help the cell respond to signals that
321 activate innate immune pathways (20,22,36,85). It is not clear if PB antiviral activities are
322 connected to established regulators of innate immune signaling such as the RNA sensors RIG-
323 I/MDA5, transcription factors IRF3/NF-kB, or the production of Type I IFNs, though reports
324 suggest this may indeed be the case (36,85,87). The recent demonstration that TRAF6 controls
325 Dcp1a localization within PBs using ubiquitylation suggests that antiviral signaling is more
326 complex than previously appreciated and integrates transcriptional responses with cytokine
327 mRNA suppression in PBs (85,87). Moreover, the PB protein Lsm14A has also been shown to
328 bind to viral RNA/DNA after infection to promote IRF3 activation and IFN-β production (36).
329 Although it remains unclear if organization of particular proteins in PBs, or the higher order
330 condensation of many proteins into the PB, regulates its antiviral activity (82,87), what is clear is
331 that PB disassembly reverses the constitutive decay or translational suppression of cytokine
332 mRNAs that contain AREs that would normally occur there (11-15,88). These data suggest that

333 when viruses coordinate an attack to cause PB loss, this event relieves the cytokine mRNA
334 suppression and acts as a danger signal that signals the immune system for help. In this way, PB
335 disassembly may be a central component of the cellular innate immune response and part of the
336 sequelae of signals that notify the immune system that a cell is infected. In situations where
337 interferon responses are delayed or defective, as is emerging for SARS-CoV-2 and severe
338 COVID (45-53), PB disassembly may be an important contributing factor to pathogenic cytokine
339 responses. Therefore, in part two of our model, we propose that cells view viral PB disassembly
340 as a danger signal and respond by increasing production of proinflammatory cytokines as a call
341 for reinforcements.
342
343 A new model for the role of PBs as a nexus of intracellular antiviral responses
344 We now propose a model for how PBs may regulate cellular innate responses to CoV infection
345 (Fig 6). Our model places PBs at a nexus point, a connection between intracellular direct-acting
346 antiviral responses and proinflammatory cytokine responses. We propose that PBs function as
347 direct-acting antiviral granules that can restrict virus infection if robustly induced into phase-
348 separated molecular condensates; for this reason, they are targeted by disassembly by most
349 viruses. Second, when viral invaders cause PB loss, the cell responds to the inactivation of PBs
350 with a call for reinforcements. This occurs because PBs house suppressed cytokine transcripts
351 which are relieved of their suppression by viral PB disassembly. This model places the PB as a
352 central player in the antiviral response that coordinates the immune reshaping that occurs after
353 CoV infection.
354
355
356
357
358
359
360

361 **Materials and Methods**

362 **Cell culture**

363 All cells were maintained at 37 °C with 5% CO_2 and 20% O_2. Vero E6 (ATCC), HEK293T cells
364 (ATCC), HeLa Tet-Off cells (Clontech) and HeLa Flp-In TREx GFP-Dcp1a cells (a generous
365 gift from Anne-Claude Gingras (6)) were cultured in DMEM (Thermo Fisher) supplemented
366 with 100 U/mL penicillin, 100 µg/mL streptomycin, 2 mM L-glutamine (Thermo Fisher) and
367 10% FBS (Thermo Fisher). HUVECs (Lonza) were cultured in endothelial cell growth medium
368 (EGM-2) (Lonza). HUVECs were seeded onto gelatin-coated tissue culture plates or glass
369 coverslips.

370 **Plasmids and Cloning**

371 pLenti-IRES-Puro SARS-CoV2 plasmids were a generous gift from the Krogan Lab (89).
372 pLJM1-GFP-Dcp1a was generated by cloning pT7-EGFP-C1-HsDCP1a (Addgene 25030) into
373 pLJM1-BSD (90)using AgeI and SmaI restriction sites (NEB). pLJM1-KapB-BSD was
374 generated by cloning pBMNIP-KapB (13) into pLJM1-BSD using EcoRI and BamHI restriction
375 sites (NEB).

376 **Transient Transfections**

377 Transient transfections were performed using Fugene (Promega) according to manufacturer's
378 guidelines. Briefly, HeLa Flp-In TREx GFP-Dcp1a cells were seeded in 12-well plates at
379 150,000 cells/well in antibiotic-free DMEM on coverslips for immunofluorescence or directly in
380 wells for lysates. Cells were transfected with 1 µg of DNA and 3 µL of Fugene for 48 h before
381 processing.

382 **Lentivirus generation**

383 All lentiviruses were generated using a second-generation system. Briefly, HEK293T cells were
384 transfected with pSPAX2, MD2G, and the plasmid containing a gene of interest using
385 polyethylimine (PEI, Polysciences). Viral supernatants were harvested 48 h post-transfection
386 and frozen at -80°C until use. For transduction, lentiviruses were thawed at 37°C and added to
387 target cells in complete media containing 5 µg/mL polybrene (Sigma) for 24 h. The media was
388 changed to selection media containing 1 µg/mL puromycin or 5 µg/mL blasticidin (Thermo
389 Fisher) and cells were selected for 48 hours before proceeding with experiments.

390 **Immunofluorescence**

391 Cells were seeded onto coverslips for immunofluorescence experiments. Following treatment,
392 cells were fixed for 10 mins at 37 °C in 4% (v/v) paraformaldehyde (Electron Microscopy
393 Sciences). Samples were permeabilized with 0.1% (v/v) Triton X-100 (Sigma-Aldrich) for 10
394 min at room temperature and blocked in 1% human AB serum (Sigma-Aldrich) 1 h at room
395 temperature. Primary and secondary antibodies were diluted in 1% human AB serum and used at
396 the concentrations in Table 1. Nuclei were stained with DAPI. Samples were mounted with
397 Prolong Gold AntiFade mounting media (Thermo).

398 **Immunoblotting**

399 Cells were lysed in 2X Laemmli buffer and stored at -20°C until use. The DC Protein Assay
400 (Bio-Rad) was used to quantify protein concentration as per the manufacturer's instructions. 10-
401 15 µg of protein lysate was resolved by SDS-PAGE on 4-15% gradient TGX Stain-Free
402 acrylamide gels (BioRad). Total protein images were acquired from the PVDF membranes after
403 transfer on the ChemiDoc Touch Imaging system (BioRad). Membranes were blocked in 5%
404 BSA in TBS-T. Primary and secondary antibodies were diluted in 2.5% BSA, and used at the
405 dilutions found in Table 1. Membranes were visualized using Clarity Western ECL substrate and
406 the ChemiDoc Touch Imaging system (BioRad).

407 **Luciferase Assays**

408 HeLa Tet-Off cells were transfected according to Corcoran J.A. et al. *Methods* (2011) with
409 pTRE2-Firefly Luciferase-ARE, pTRE2-Renilla Luciferase, and SARS-CoV2 plasmids using
410 Fugene HD (Promega). Firefly and Renilla luciferase activity were quantified using the Dual
411 Luciferase Assay Kit (Promega) and read on a Modulus Microplate luminometer (Promega).

412 **Quantitative PCR**

413 RNA was collected using an RNeasy Plus Mini Kit (Qiagen) according to the manufacturer's
414 instructions and stored at -80°C until use. RNA concentration was determined and was reverse
415 transcribed using qScript XLT cDNA SuperMix (QuantaBio) using a combination of random
416 hexamer and oligo dT primers, according to the manufacturer's instructions. Depending on
417 starting concentration, cDNA was diluted between 1:10 and 1:20 for qPCR experiments and
418 SsoFast EvaGreen Mastermix (Biorad) was used to amplify cDNA. The ΔΔquantitation cycle
419 (Cq) method was used to determine the fold change in expression of target transcripts. qPCR
420 primer sequences can be found in Table 2

421 **OC43-CoV Propagation and Infection**

422 Stocks of hCoV-OC43 (ATCC) were propagated in Vero E6 cells. To produce viral stocks, Vero
423 E6 cells were infected at an MOI of 0.01 for 1 h in serum-free DMEM at 33˚C. Following
424 infection, the viral inoculum was removed and replaced with DMEM supplemented with 2%
425 heat-inactivated FBS and 100 units/mL penicillin/streptomycin/glutamine. After 6 days, the
426 supernatant was harvested and centrifuged at 2000 RPM for 5 mins to remove cellular debris.
427 Virus stocks were aliquoted and stored at -80˚C for single use. Viral titers were enumerated
428 using Reed and Muench tissue-culture infectious dose 50% (TCID50) in Vero E6 cells (64). For
429 infection, cells were seeded onto coverslips to achieve ~70% confluency after 24 hours. The
430 following day, the growth media was removed and replaced with 100 µl of human CoV-OC43
431 inoculum and incubated at 37˚C for one hour, rocking the plate every 10 minutes to distribute
432 viral inoculum. Following incubation, the virus inoculum was removed and replaced with EGM-
433 2.
434
435 **Processing Body Quantification**
436 Processing bodies were quantified using an unbiased image analysis pipeline generated in the
437 freeware CellProfiler (cellprofiler.org) (91). First, detection of nuclei in the DAPI channel image
438 was performed by applying a binary threshold and executing primary object detection between
439 50 and 250 pixels. From each identified nuclear object, the "Propagation" function was
440 performed on the respective CoV2-ORF channel image to define cell borders. The identified cell
441 borders were masked with the identified nuclei to define a cytoplasm mask. The cytoplasm mask
442 was then applied to the processing body puncta channel image to ensure only cytoplasmic puncta
443 were quantified. Background staining was reduced in the cytoplasmic puncta channel using the
444 "Enhance Speckles" function. Using "global thresholding with robust background adjustments",
445 puncta within a defined size and intensity range were quantified. Size and intensity thresholds
446 were unchanged between experiments with identical staining parameters. Intensity measurements
447 of puncta and CoV2-ORF staining were quantified. Quantification data was exported and
448 RStudio was used for data analysis.
449
450 **Statistics**
451 All statistical analyses were performed using GraphPad Prism 8.0. Significance was determined
452 using the tests indicated in each of the figure legends.

453 **Figure Legends**

454 Figure 1: A screen of SARS-CoV2 genes reveals mediators of processing body loss. A: HeLa
455 Flp-In TREx GFP-Dcp1a cells were transfected with an empty vector or 2xStrep-tagged SARS-
456 CoV2 ORFs for 48 h and then fixed and immunostained for Strep-tag (red), DDX6 (white), and
457 nuclei (blue). Select ORFs are shown; Scale bar=20 µm. B: DDX6 puncta were quantified using
458 CellProfiler on SARS-CoV2 ORF-expressing cells thresholded by Strep-tag staining intensity.
459 The intensity threshold used to determine ORF-expressing cells was defined as two standard
460 deviations above mean intensity in vector controls. Values are expressed as a fold-change
461 difference normalized to the vector control (hashed line). A one-way ANOVA with a Dunnett's
462 post-hoc analysis was performed, n=3; bars represent SEM; **=P<0.01. C: Lysates were
463 harvested from HeLas transfected with 2xStrep-tagged SARS-CoV2 ORFs after 48 h of
464 expression in 2x Laemmli buffer. Samples were resolved by SDS-PAGE on 4-15% gradient gels
465 (BioRad) and immunoblotted with a Strep-Tag II antibody (Sigma).

466

467 Figure 2: ARE-mRNA stability is affected by SARS-CoV2 gene expression. A: Schematic of
468 luciferase constructs used for ARE-mRNA stability assay. Both firefly and renilla luciferase are
469 under the control of a promoter that is inhibited in the presence of doxycycline. The firefly
470 luciferase construct contains an AU-rich element (ARE) in its 3' UTR, targeting it for
471 degradation in the presence of processing bodies. B: HeLa Tet-Off cells were transfected with
472 both the firefly (FLuc) and renilla (RLuc) luciferase constructs with either an empty vector,
473 kaposin B (KapB, positive control), or the SARS-CoV2 genes. Doxycycline was added 36 h
474 post-transfection to stop expression of luciferase constructs from TRE2 promoters and cells were
475 lysed at 48 h post-transfection. Firefly and renilla luminescence were measured using a Dual
476 Luciferase Reporter Assay System (Promega) and a Modulus Microplate (Promega). Values are
477 reported as firefly luminescence/renilla luminescence normalized to the empty vector control. A
478 one-way ANOVA with a Dunnett's post-hoc analysis was performed, n=3; bars represent SEM;
479 ****=P<0.0001; # nsp1 caused low renilla luciferase values resulting in an artificially high
480 firefly/renilla value.

481

482 Figure 3: SARS-CoV2 genes induce processing body disassembly in primary endothelial cells.
483 A: Human umbilical vein endothelial cells (HUVECs) were transduced with selected 2xStrep-

484 tagged SARS-CoV2 ORFs or an empty vector control and selected with puromycin for 48 h.
485 Samples were fixed and immunostained for Strep-tag (red), DDX6 (white), and nuclei (blue).
486 Scale bar=20 μm. B: DDX6 puncta were quantified using CellProfiler on the images in A.
487 Values are expressed as a fold-change difference normalized to the empty vector control (hashed
488 line). n=2, bars indicate ranges. C: HeLa Flp-In TREx GFP-Dcp1a cells were transfected with
489 SARS-CoV2 nsp14 and fixed 48 h post-transfection. Samples were immunostained for Strep-tag
490 (white) and DDX6 (red). White arrows indicate overlapping staining.
491
492 Figure 4: Human coronavirus OC43 disassembles processing bodies in primary endothelial cells.
493 A: HUVECs were infected with OC43 (viral stock of $3.5x10^4$ TCID50/mL). Samples were fixed
494 at the indicated times post-infection and stained for OC43-N protein (green), DDX6 (white), and
495 nuclei (blue). Scale bar=20 μm. B: Using images from A, DDX6 puncta in mock or OC43
496 infected cells were quantified using CellProfiler. Values are represented as fold-change relative
497 to mock (hashed line). A one-way ANOVA with a Dunnett's post-hoc analysis was performed,
498 n=3; bars represent SEM; *=P<0.05. C: RT-qPCR was performed for ARE-mRNAs, IL-6 and
499 IL-8, on OC43 infected HUVECs at 24 hpi. n=3; bars represent geometric SD.
500
501 Figure 5: Overexpression of GFP-Dcp1a restricts OC43 infection. A: HUVECs were transduced
502 with lentiviruses expressing either a GFP-control or GFP-Dcp1a prior to being infected with
503 OC43 (with a viral stock of $3.5x10^4$ TCID50/mL). Samples were fixed at 6, 12, and 24 hpi (only
504 6 and 24 hpi shown) and stained for OC43-N protein (red) and nuclei (blue). Scale bar=20 μm.
505 B: Using images from A, infected and uninfected cells were quantified at 6, 12, and 24 hpi.
506 Values are represented as fold-change relative to the paired GFP control for each time point. For
507 6 hpi, n=2; for 12 and 24 hpi n=3. C: Supernatants were harvested at 24 hpi and titrated on naive
508 Vero E6 cells using TCID50. n=2.
509
510 Figure 6: Processing bodies are a nexus point for virus-host conflict. In part one of our model,
511 we hypothesize that PBs are direct-acting antiviral granules that can restrict virus infection when
512 present as visible condensates; for this reason, they are targeted for disassembly by most viruses.
513 In part two of our model, we propose that viral PB disassembly is perceived by the cell as a
514 danger signal and relieves suppressed cytokine transcripts to produce proinflammatory cytokines

515 that recruit and activate immune cells. In this way, PB disassembly may also contribute to the
516 pathogenic cytokine responses that underly many viral illnesses including COVID.
517
518 Figure S1: Hedls/Edc4 staining colocalizes with GFP-Dcp1a puncta to visualize processing
519 bodies. HeLa Flp-In TREx GFP-Dcp1a cells were induced with 1 μg/mL doxycycline for 24 h.
520 Samples were fixed and immunostained for the PB resident protein Hedls/Edc4 (red). Scale
521 bar=20 μm.
522
523

524

525 Table 1: Antibodies

Antibody	Species	Vendor/Catalog #	Application	Dilution
Strep-Tag II	Mouse	Sigma (71590-M)	Immunofluorescence Immunoblot	1:1000 1:1000
DDX6	Rabbit	Bethyl (A300-461)	Immunofluorescence	1:1000
Coronavirus OC43	Mouse	Millipore (MAB9012)	Immunofluorescence	1:500
Alexa Fluor 555-donkey anti-mouse	Donkey	Thermo Fisher (A31570)	Immunofluorescence Secondary	1:1000
Alexa Fluor 555-donkey anti-rabbit	Donkey	Thermo Fisher (A31572)	Immunofluorescence Secondary	1:1000
Alexa Fluor 488-chicken anti-mouse	Chicken	Thermo Fisher (A21200)	Immunofluorescence Secondary	1:1000
Alexa Fluor 488-chicken anti-rabbit	Chicken	Thermo Fisher (A21441)	Immunofluorescence Secondary	1:1000
Alexa Fluor 647-chicken anti-mouse	Chicken	Thermo Fisher (A21463)	Immunofluorescence Secondary	1:1000

526

527 Table 2: RT-qPCR primers

528

Target	Direction	Sequence 5'-3'
HPRT	Forward	CTTTCCTTGGTCAGGCAGTATAA
HPRT	Reverse	AGTCTGGCTTATATCCAACACTTC
18S	Forward	TTCGAACGTCTGCCCTATCAA
18S	Reverse	GATGTGGTAGCCGTTTCTCAGG
B2M	Forward	TTTCCATTCTCTGCTGGATGAC
B2M	Reverse	TGCTGTCTCCATGTTTGATGTA
IL6	Forward	GTCCAGTTGCCTTCTCCCTGG
IL6	Reverse	GAGATGCCGTCGAGGATGTACC
CXCL8	Forward	AAATCTGGCAACCCTAGTCTG
CXCL8	Reverse	GTGAGGTAAGATGGTGGCTAAT
IL-1β	Forward	CTCTCACCTCTCCTACTCACTT
IL-1β	Reverse	TCAGAATGTGGGAGCGAATG
TNF	Forward	TCGAACCCCGAGTGACAA
TNF	Reverse	AGCTGCCCCTCAGCTTG
GM-CSF	Forward	AAATGTTTGACCTCCAGGAGCC
GM-CSF	Reverse	ATCTGGGTTGCACAGGAAGTT
COX-2	Forward	CCCTTGGGTGTCAAAGGTAA
COX-2	Reverse	GCCCTCGCTTATGATCTGTC
VEGF	Forward	CGAGACCTTGGTGGACATC
VEGF	Reverse	CTGCATGGTGACGTTGAAC

529

530 Table 3: Plasmids

Plasmid Name	Use	Source	Mammalian Selection
pLJM1-BSD	Empty vector control	(90)	Blasticidin
pLJM1-KapB-BSD	Positive control	Cloned from pBMNIP-KapB (13) into pLJM1-BSD	Blasticidin
pLJM1-GFP-DCP1a-BSD	Overexpression	Cloned from pT7-EGFP-C1-HsDCP1a (Addgene 25030) into pLJM1-BSD	Blasticidin
pLenti-SARS-CoV2-IRES-Puro	Overexpression library	(89)	Puromycin
pTwist-SARS-CoV2-Spike-IRES-Puro	Overexpression	(89)	Puromycin
pTRE2-Firefly Luciferase-ARE	ARE-mRNA stability	(59)	N/A
pTRE2-Renilla Luciferase	ARE-mRNA stability	(59)	N/A
pMD2.G	Lentivirus generation	Addgene 12259	N/A
psPAX2	Lentivirus generation	Addgene 12260	N/A

531
532
533
534

535 **References**

536

537 1. Cougot N, Cavalier A, Thomas D, Gillet R. The dual organization of P-bodies revealed by
538 immunoelectron microscopy and electron tomography. J Mol Biol. 2012 Jun 29;420(1-
539 2):17–28.

540 2. Hubstenberger A, Courel M, Bénard M, Souquere S, Ernoult-Lange M, Chouaib R, et al.
541 P-Body Purification Reveals the Condensation of Repressed mRNA Regulons. Mol Cell.
542 Elsevier Inc; 2017 Oct 5;68(1):144–5.

543 3. Corbet GA, Parker R. RNP Granule Formation: Lessons from P-Bodies and Stress
544 Granules. Cold Spring Harb Symp Quant Biol. 2019;84:203–15.

545 4. Riggs CL, Kedersha N, Ivanov P, Anderson P. Mammalian stress granules and P bodies at
546 a glance. J Cell Sci. 2020 Sep 1;133(16):jcs242487.

547 5. Tibble RW, Depaix A, Kowalska J, Jemielity J, Gross JD. Biomolecular condensates
548 amplify mRNA decapping by coupling protein interactions with conformational changes
549 in Dcp1/Dcp2. 2020 Jul 9;60th Anniversary(479–480):600–36.

550 6. Youn J-Y, Dunham WH, Hong SJ, Knight JDR, Bashkurov M, Chen GI, et al. High-
551 Density Proximity Mapping Reveals the Subcellular Organization of mRNA-Associated
552 Granules and Bodies. Mol Cell. 2018 Feb 1;69(3):517–532.e11.

553 7. Khong A, Parker R. mRNP architecture in translating and stress conditions reveals an
554 ordered pathway of mRNP compaction. J Cell Biol. 2018 Oct 15;217(12):4124–40.

555 8. Matheny T, Rao BS, Parker R. Transcriptome-Wide Comparison of Stress Granules and
556 P-Bodies Reveals that Translation Plays a Major Role in RNA Partitioning. Mol Cell Biol.
557 2019 Dec 15;39(24):612.

558 9. Bakheet T, Hitti E, Khabar KSA. ARED-Plus: an updated and expanded database of AU-
559 rich element-containing mRNAs and pre-mRNAs. Nucleic Acids Research. 2018 Jan
560 4;46(D1):D218–20.

561 10. Hitti E, Bakheet T, Al-Souhibani N, Moghrabi W, Al-Yahya S, Al-Ghamdi M, et al.
562 Systematic Analysis of AU-Rich Element Expression in Cancer Reveals Common
563 Functional Clusters Regulated by Key RNA-Binding Proteins. Cancer Res. 2016 Jul
564 15;76(14):4068–80.

565 11. Blanco FF, Sanduja S, Deane NG, Blackshear PJ, Dixon DA. Transforming growth factor
566 β regulates P-body formation through induction of the mRNA decay factor tristetraprolin.
567 Mol Cell Biol. 2014 Jan;34(2):180–95.

568 12. Corcoran JA, Khaperskyy DA, Johnston BP, King CA, Cyr DP, Olsthoorn AV, et al.
569 Kaposi's sarcoma-associated herpesvirus G-protein-coupled receptor prevents AU-rich-
570 element-mediated mRNA decay. J Virol. 2012 Aug;86(16):8859–71.

571 13. Corcoran JA, Johnston BP, McCormick C. Viral Activation of MK2-hsp27-p115RhoGEF-
572 RhoA Signaling Axis Causes Cytoskeletal Rearrangements, P-body Disruption and ARE-
573 mRNA Stabilization. Robertson ES, editor. PLoS Pathogens. Public Library of Science;
574 2015 Jan 8;11(1):e1004597.

575 14. Franks TM, Lykke-Andersen J. TTP and BRF proteins nucleate processing body
576 formation to silence mRNAs with AU-rich elements. Genes Dev. 2007 Mar 15;21(6):719–
577 35.

578 15. Vindry C, Marnef A, Broomhead H, Twyffels L, Ozgur S, Stoecklin G, et al. Dual RNA
579 Processing Roles of Pat1b via Cytoplasmic Lsm1-7 and Nuclear Lsm2-8 Complexes.
580 CellReports. 2017 Aug 1;20(5):1187–200.

581 16. Corcoran JA, McCormick C. Viral activation of stress-regulated Rho-GTPase signaling
582 pathway disrupts sites of mRNA degradation to influence cellular gene expression. Small
583 GTPases. Taylor & Francis; 2015 Oct 2;6(4):178–85.

584 17. Standart N, Weil D. P-Bodies: Cytosolic Droplets for Coordinated mRNA Storage. Trends
585 Genet. 2018 Aug;34(8):612–26.

586 18. Docena G, Rovedatti L, Kruidenier L, Fanning A, Leakey NAB, Knowles CH, et al.
587 Down-regulation of p38 mitogen-activated protein kinase activation and proinflammatory
588 cytokine production by mitogen-activated protein kinase inhibitors in inflammatory bowel
589 disease. Clin Exp Immunol. John Wiley & Sons, Ltd; 2010 Oct;162(1):108–15.

590 19. Jangra RK, Yi M, Lemon SM. DDX6 (Rck/p54) is required for efficient hepatitis C virus
591 replication but not for internal ribosome entry site-directed translation. J Virol. 2010
592 Jul;84(13):6810–24.

593 20. Ng CS, Kasumba DM, Fujita T, Luo H. Spatio-temporal characterization of the antiviral
594 activity of the XRN1-DCP1/2 aggregation against cytoplasmic RNA viruses to prevent
595 cell death. Cell Death & Differentiation. Nature Publishing Group; 2020 Feb 7;36:932–20.

596 21. Ostareck DH, Naarmann-de Vries IS, Ostareck-Lederer A. DDX6 and its orthologs as
597 modulators of cellular and viral RNA expression. Wiley Interdiscip Rev RNA. 2014
598 Sep;5(5):659–78.

599 22. Dougherty JD, Tsai W-C, Lloyd RE. Multiple Poliovirus Proteins Repress Cytoplasmic
600 RNA Granules. Viruses. Multidisciplinary Digital Publishing Institute; 2015 Nov
601 25;7(12):6127–40.

602 23. Dougherty JD, White JP, Lloyd RE. Poliovirus-mediated disruption of cytoplasmic
603 processing bodies. J Virol. 2011 Jan;85(1):64–75.

604 24. Gaete-Argel A, Márquez CL, Barriga GP, Soto-Rifo R, Valiente-Echeverría F. Strategies
605 for Success. Viral Infections and Membraneless Organelles. Front Cell Infect Microbiol.
606 2019;9:336.

607 25. McCormick C, Khaperskyy DA. Translation inhibition and stress granules in the antiviral
608 immune response. Nature Reviews Immunology. Nature Publishing Group; 2017
609 Oct;17(10):647–60.

610 26. Tsai W-C, Lloyd RE. Cytoplasmic RNA Granules and Viral Infection. Annu Rev Virol.
611 Annual Reviews; 2014 Nov;1(1):147–70.

612 27. Onomoto K, Jogi M, Yoo J-S, Narita R, Morimoto S, Takemura A, et al. Critical role of
613 an antiviral stress granule containing RIG-I and PKR in viral detection and innate
614 immunity. Kanai A, editor. PLoS ONE. Public Library of Science; 2012;7(8):e43031.

615 28. Abernathy E, Glaunsinger B. Emerging roles for RNA degradation in viral replication and
616 antiviral defense. Virology. 2015 May;479-480:600–8.

617 29. Núñez RD, Budt M, Saenger S, Paki K, Arnold U, Sadewasser A, et al. The RNA
618 Helicase DDX6 Associates with RIG-I to Augment Induction of Antiviral Signaling. Int J
619 Mol Sci. Multidisciplinary Digital Publishing Institute; 2018 Jun 26;19(7):1877.

620 30. Balinsky CA, Schmeisser H, Wells AI, Ganesan S, Jin T, Singh K, et al. IRAV
621 (FLJ11286), an Interferon-Stimulated Gene with Antiviral Activity against Dengue Virus,
622 Interacts with MOV10. Diamond MS, editor. J Virol. 2017 Mar 1;91(5):504.

623 31. Wang H, Chang L, Wang X, Su A, Feng C, Fu Y, et al. MOV10 interacts with Enterovirus
624 71 genomic 5'UTR and modulates viral replication. Biochem Biophys Res Commun. 2016
625 Oct 21;479(3):571–7.

626 32. Cuevas RA, Ghosh A, Wallerath C, Hornung V, Coyne CB, Sarkar SN. MOV10 Provides
627 Antiviral Activity against RNA Viruses by Enhancing RIG-I-MAVS-Independent IFN
628 Induction. J Immunol. 2016 May 1;196(9):3877–86.

629 33. Burdick R, Smith JL, Chaipan C, Friew Y, Chen J, Venkatachari NJ, et al. P body-
630 associated protein Mov10 inhibits HIV-1 replication at multiple stages. J Virol. 2010
631 Oct;84(19):10241–53.

632 34. Burgess HM, Mohr I. Cellular 5“-3” mRNA exonuclease Xrn1 controls double-stranded
633 RNA accumulation and anti-viral responses. Cell Host and Microbe. 2015 Mar
634 11;17(3):332–44.

635 35. Lumb JH, Li Q, Popov LM, Ding S, Keith MT, Merrill BD, et al. DDX6 Represses
636 Aberrant Activation of Interferon- Stimulated Genes. CellReports. ElsevierCompany;
637 2017 Jul 25;20(4):819–31.

638 36. Li Y, Chen R, Zhou Q, Xu Z, Li C, Wang S, et al. LSm14A is a processing body-
639 associated sensor of viral nucleic acids that initiates cellular antiviral response in the early
640 phase of viral infection. Proc Natl Acad Sci USA. 2012 Jul 17;109(29):11770–5.

641 37. V'kovski P, Kratzel A, Steiner S, Stalder H, Thiel V. Coronavirus biology and replication:
642 implications for SARS-CoV-2. Nat Rev Microbiol. Nature Publishing Group; 2020 Oct
643 28;5:536–16.

644 38. Cui J, Li F, Shi Z-L. Origin and evolution of pathogenic coronaviruses. Springer US; 2019
645 Feb 6;:1–12.

646 39. Fielding CA, Jones GW, McLoughlin RM, McLeod L, Hammond VJ, Uceda J, et al.
647 Interleukin-6 signaling drives fibrosis in unresolved inflammation. Immunity. 2014 Jan
648 16;40(1):40–50.

649 40. Blanco-Melo D, tenover BR. Imbalanced host response to SARS-CoV-2 drives
650 development of COVID-19. Cell. 2020 Apr 15;:1–46.

651 41. Chen G, Wu D, Guo W, Cao Y, Huang D, Wang H, et al. Clinical and immunological
652 features of severe and moderate coronavirus disease 2019. J Clin Invest. American Society
653 for Clinical Investigation; 2020 May 1;130(5):2620–9.

654 42. Pedersen SF, Ho Y-C. SARS-CoV-2: a storm is raging. Journal of Clinical Investigation.
655 2020 Mar 23;130(5):2202–5.

656 43. Andersen KG, Rambaut A, Lipkin WI, Holmes EC, Garry RF. The proximal origin of
657 SARS-CoV-2. Nature Medicine. 2020 Mar 17;26(4):450–2.

658 44. Zou L, Ruan F, Huang M, Liang L, Huang H, Hong Z, et al. SARS-CoV-2 Viral Load in
659 Upper Respiratory Specimens of Infected Patients. N Engl J Med. Massachusetts Medical
660 Society; 2020 Mar 19;382(12):1177–9.

661 45. Park A, Iwasaki A. Type I and Type III Interferons - Induction, Signaling, Evasion, and
662 Application to Combat COVID-19. Cell Host and Microbe. 2020 Jun 10;27(6):870–8.

663 46. Bastard P, Rosen LB, Zhang Q, Michailidis E, Hoffmann H-H, Zhang Y, et al. Auto-
664 antibodies against type I IFNs in patients with life-threatening COVID-19. Science. 2020
665 Sep 24;129:eabd4585.

666 47. Zhang Q, Bastard P, Liu Z, Le Pen J, Moncada-Velez M, Chen J, et al. Inborn errors of
667 type I IFN immunity in patients with life-threatening COVID-19. Science. 2020 Sep
668 24;:eabd4570.

669 48. Ackermann M, Mentzer SJ, Kolb M, Jonigk D. Inflammation and Intussusceptive
670 Angiogenesis in COVID-19: everything in and out of Flow. Eur Respir J. 2020 Oct
671 2;383:2003147.

672 49. Yuen C-K, Lam J-Y, Wong W-M, Mak L-F, Wang X, Chu H, et al. SARS-CoV-2 nsp13,
673 nsp14, nsp15 and orf6 function as potent interferon antagonists. Emerging Microbes &
674 Infections. Taylor & Francis; 2020 Dec;9(1):1418–28.

675 50. Miorin L, Kehrer T, Sanchez-Aparicio MT, Zhang K, Cohen P, Patel RS, et al. SARS-
676 CoV-2 Orf6 hijacks Nup98 to block STAT nuclear import and antagonize interferon
677 signaling. Proc Natl Acad Sci USA. 2020 Oct 23;5:202016650–11.

678 51. Li Y, Renner DM, Comar CE, Whelan JN, Reyes HM, Cardenas-Diaz FL, et al. SARS-
679 CoV-2 induces double-stranded RNA-mediated innate immune responses in respiratory
680 epithelial derived cells and cardiomyocytes. bioRxiv. 2020 Sep 25;67:4504.

681 52. Banerjee AK, Blanco MR, Bruce EA, Honson DD, Chen LM, Chow A, et al. SARS-CoV-
682 2 disrupts splicing, translation, and protein trafficking to suppress host defenses. Cell.
683 Elsevier Inc; 2020 Oct 7;:1–66.

684 53. Konno Y, Kimura I, Uriu K, Fukushi M, Irie T, Koyanagi Y, et al. SARS-CoV-2 ORF3b
685 Is a Potent Interferon Antagonist Whose Activity Is Increased by a Naturally Occurring
686 Elongation Variant. CellReports. 2020 Sep 22;32(12):108185.

687 54. Sola I, Galán C, Mateos-Gómez PA, Palacio L, Zuñiga S, Cruz JL, et al. The
688 polypyrimidine tract-binding protein affects coronavirus RNA accumulation levels and
689 relocalizes viral RNAs to novel cytoplasmic domains different from replication-
690 transcription sites. J Virol. 3rd ed. 2011 May;85(10):5136–49.

691 55. Raaben M, Groot Koerkamp MJA, Rottier PJM, de Haan CAM. Mouse hepatitis
692 coronavirus replication induces host translational shutoff and mRNA decay, with
693 concomitant formation of stress granules and processing bodies. Cellular Microbiology.
694 2007 Sep;9(9):2218–29.

695 56. Wang X, Chang L, Wang H, Su A, Wu Z. Dcp1a and GW182 Induce Distinct Cellular
696 Aggregates and Have Different Effects on microRNA Pathway. DNA and Cell Biology.
697 2017 Jul;36(7):565–70.

698 57. Gordon DE, Jang GM, Bouhaddou M, Xu J, Obernier K, O'Meara MJ, et al. A SARS-
699 CoV-2-Human Protein-Protein Interaction Map Reveals Drug Targets and Potential Drug-
700 Repurposing. 2020 Mar 22;579:265–45.

701 58. Castle EL, Douglas P, Rinker KD, Corcoran JA. Viral manipulation of a novel
702 mechanoresponsive signaling axis disassembles processing bodies. 2020 May
703 15;48(4):245–65.

704 59. Corcoran JA, Khaperskyy DA, McCormick C. Assays for monitoring viral manipulation
705 of host ARE-mRNA turnover. Methods. 2011 Oct;55(2):172–81.

706 60. Pons S, Fodil S, Azoulay E, Zafrani L. The vascular endothelium: the cornerstone of
707 organ dysfunction in severe SARS-CoV-2 infection. Crit Care. BioMed Central; 2020 Jun
708 16;24(1):353–8.

709 61. Varga Z, Flammer AJ, Steiger P, Haberecker M, Andermatt R, Zinkernagel AS, et al.
710 Endothelial cell infection and endotheliitis in COVID-19. Elsevier Ltd; 2020 Apr 17;:1–2.

711 62. Libby P, Lüscher T. COVID-19 is, in the end, an endothelial disease. Eur Heart J. 3rd ed.
712 2020 Sep 1;41(32):3038–44.

713 63. Lowenstein CJ, Solomon SD. Severe COVID-19 is a Microvascular Disease. Circulation.
714 Lippincott Williams & Wilkins Hagerstown, MD; 2020 Sep 2;191:148.

715 64. Ramakrishnan MA. Determination of 50% endpoint titer using a simple formula. World J
716 Virol. 2016 May 12;5(2):85–6.

717 65. Cong Y, Ulasli M, Schepers H, Mauthe M, V'kovski P, Kriegenburg F, et al.
718 Nucleocapsid Protein Recruitment to Replication-Transcription Complexes Plays a
719 Crucial Role in Coronaviral Life Cycle. Dutch RE, editor. J Virol. American Society for
720 Microbiology Journals; 2020 Jan 31;94(4):181.

721 66. Lu S, Ye Q, Singh D, Villa E, Cleveland DW, Corbett KD. The SARS-CoV-2
722 Nucleocapsid phosphoprotein forms mutually exclusive condensates with RNA and the
723 membrane-associated M protein. bioRxiv. 2020 Jul 31;18(6):479.

724 67. Cascarina SM, Ross ED. A proposed role for the SARS-CoV-2 nucleocapsid protein in
725 the formation and regulation of biomolecular condensates. FASEB j. 2020 Jun
726 20;34(8):9832–42.

727 68. McBride R, van Zyl M, Fielding BC. The coronavirus nucleocapsid is a multifunctional
728 protein. Viruses. Multidisciplinary Digital Publishing Institute; 2014 Aug 7;6(8):2991–
729 3018.

730 69. Peng T-Y, Lee K-R, Tarn W-Y. Phosphorylation of the arginine/serine dipeptide-rich
731 motif of the severe acute respiratory syndrome coronavirus nucleocapsid protein
732 modulates its multimerization, translation inhibitory activity and cellular localization.
733 FEBS J. John Wiley & Sons, Ltd; 2008 Aug;275(16):4152–63.

734 70. Gussow AB, Auslander N, Faure G, Wolf YI, Zhang F, Koonin EV. Genomic
735 determinants of pathogenicity in SARS-CoV-2 and other human coronaviruses. Proc Natl
736 Acad Sci USA. 2020 Jun 30;117(26):15193–9.

737 71. Verheije MH, Hagemeijer MC, Ulasli M, Reggiori F, Rottier PJM, Masters PS, et al. The
738 coronavirus nucleocapsid protein is dynamically associated with the replication-
739 transcription complexes. J Virol. 2010 Nov;84(21):11575–9.

740 72. Robson F, Khan KS, Le TK, Paris C, Demirbag S, Barfuss P, et al. Coronavirus RNA
741 Proofreading: Molecular Basis and Therapeutic Targeting. Mol Cell. 2020 Sep
742 3;79(5):710–27.

743 73. Becares M, Pascual-Iglesias A, Nogales A, Sola I, Enjuanes L, Zuñiga S. Mutagenesis of
744 Coronavirus nsp14 Reveals Its Potential Role in Modulation of the Innate Immune
745 Response. Perlman S, editor. J Virol. 3rd ed. 2016 May 12;90(11):5399–414.

746 74. Rao S, Hoskins I, Garcia PD, Tonn T, Ozadam H, Cenik ES, et al. Genes with 5′ terminal
747 oligopyrimidine tracts preferentially escape global suppression of translation by the
748 SARS-CoV-2 NSP1 protein. 2020 Sep 13;48:D166–70.

749 75. Schubert K, Karousis ED, Jomaa A, Scaiola A, Echeverria B, Gurzeler L-A, et al. SARS-
750 CoV-2 Nsp1 binds the ribosomal mRNA channel to inhibit translation. Springer US; 2020
751 Sep 4;:1–19.

752 76. Fung T, Liao Y, Liu D. Regulation of Stress Responses and Translational Control by
753 Coronavirus. Viruses. 2016 Jul;8(7):184–15.

754 77. Gaglia MM, Covarrubias S, Wong W, Glaunsinger BA. A common strategy for host RNA
755 degradation by divergent viruses. J Virol. 2012 Sep;86(17):9527–30.

756 78. Narayanan K, Huang C, Lokugamage K, Kamitani W, Ikegami T, Tseng C-TK, et al.
757 Severe acute respiratory syndrome coronavirus nsp1 suppresses host gene expression,
758 including that of type I interferon, in infected cells. J Virol. 2008 May;82(9):4471–9.

759 79. Khaperskyy DA, Schmaling S, Larkins-Ford J, McCormick C, Gaglia MM. Selective
760 Degradation of Host RNA Polymerase II Transcripts by Influenza A Virus PA-X Host
761 Shutoff Protein. Palese P, editor. PLoS Pathogens. 2016 Feb;12(2):e1005427.

762 80. Schaecher SR, Touchette E, Schriewer J, Buller RM, Pekosz A. Severe Acute Respiratory
763 Syndrome Coronavirus Gene 7 Products Contribute to Virus-Induced Apoptosis. J Virol.
764 2007 Oct 15;81(20):11054–68.

765 81. Zhu X, Chen J, Tian L, Zhou Y, Xu S, Long S, et al. Porcine Deltacoronavirus nsp5
766 Cleaves DCP1A To Decrease Its Antiviral Activity. Gallagher T, editor. J Virol. American
767 Society for Microbiology Journals; 2020 Jul 16;94(15):128.

768 82. Dougherty JD, Reineke LC, Lloyd RE. mRNA decapping enzyme 1a (Dcp1a)-induced
769 translational arrest through protein kinase R (PKR) activation requires the N-terminal
770 enabled vasodilator-stimulated protein homology 1 (EVH1) domain. J Biol Chem. 2014
771 Feb 14;289(7):3936–49.

772 83. Eulalio A, Behm-Ansmant I, Izaurralde E. P bodies: at the crossroads of post-
773 transcriptional pathways. Nat Rev Mol Cell Biol. Nature Publishing Group; 2007
774 Jan;8(1):9–22.

775 84. Ayache J, Bénard M, Ernoult-Lange M, Minshall N, Standart N, Kress M, et al. P-body
776 assembly requires DDX6 repression complexes rather than decay or Ataxin2/2L
777 complexes. Matera AG, editor. Mol Biol Cell. The American Society for Cell Biology;
778 2015 Jul 15;26(14):2579–95.

779 85. Tenekeci U, Poppe M, Beuerlein K, Buro C, Müller H, Weiser H, et al. K63-
780 Ubiquitylation and TRAF6 Pathways Regulate Mammalian P-Body Formation and
781 mRNA Decapping. Mol Cell. 2016 Jun 16;62(6):943–57.

782 86. Sheth U, Parker R. Decapping and decay of messenger RNA occur in cytoplasmic
783 processing bodies. Science. American Association for the Advancement of Science; 2003
784 May 2;300(5620):805–8.

785 87. Rzeczkowski K, Beuerlein K, Müller H, Dittrich-Breiholz O, Schneider H, Kettner-
786 Buhrow D, et al. c-Jun N-terminal kinase phosphorylates DCP1a to control formation of P
787 bodies. J Cell Biol. 2011 Aug 22;194(4):581–96.

788 88. Stoecklin G, Mayo T, Anderson P. ARE-mRNA degradation requires the 5"-3" decay
789 pathway. EMBO Rep. 2006 Jan;7(1):72–7.

790 89. Gordon DE, Jang GM, Bouhaddou M, Xu J, Obernier K, O'Meara MJ, et al. A SARS-
791 CoV-2-Human Protein-Protein Interaction Map Reveals Drug Targets and Potential Drug-
792 Repurposing. 2020 Mar 22;579:265–45.

793 90. Johnston BP, Pringle ES, McCormick C. KSHV activates unfolded protein response
794 sensors but suppresses downstream transcriptional responses to support lytic replication.
795 Swaminathan S, editor. PLoS Pathogens. 2019 Dec;15(12):e1008185.

796 91. Kamentsky L, Jones TR, Fraser A, Bray M-A, Logan DJ, Madden KL, et al. Improved
797 structure, function and compatibility for CellProfiler: modular high-throughput image
798 analysis software. Bioinformatics. 2011 Apr 15;27(8):1179–80.

799

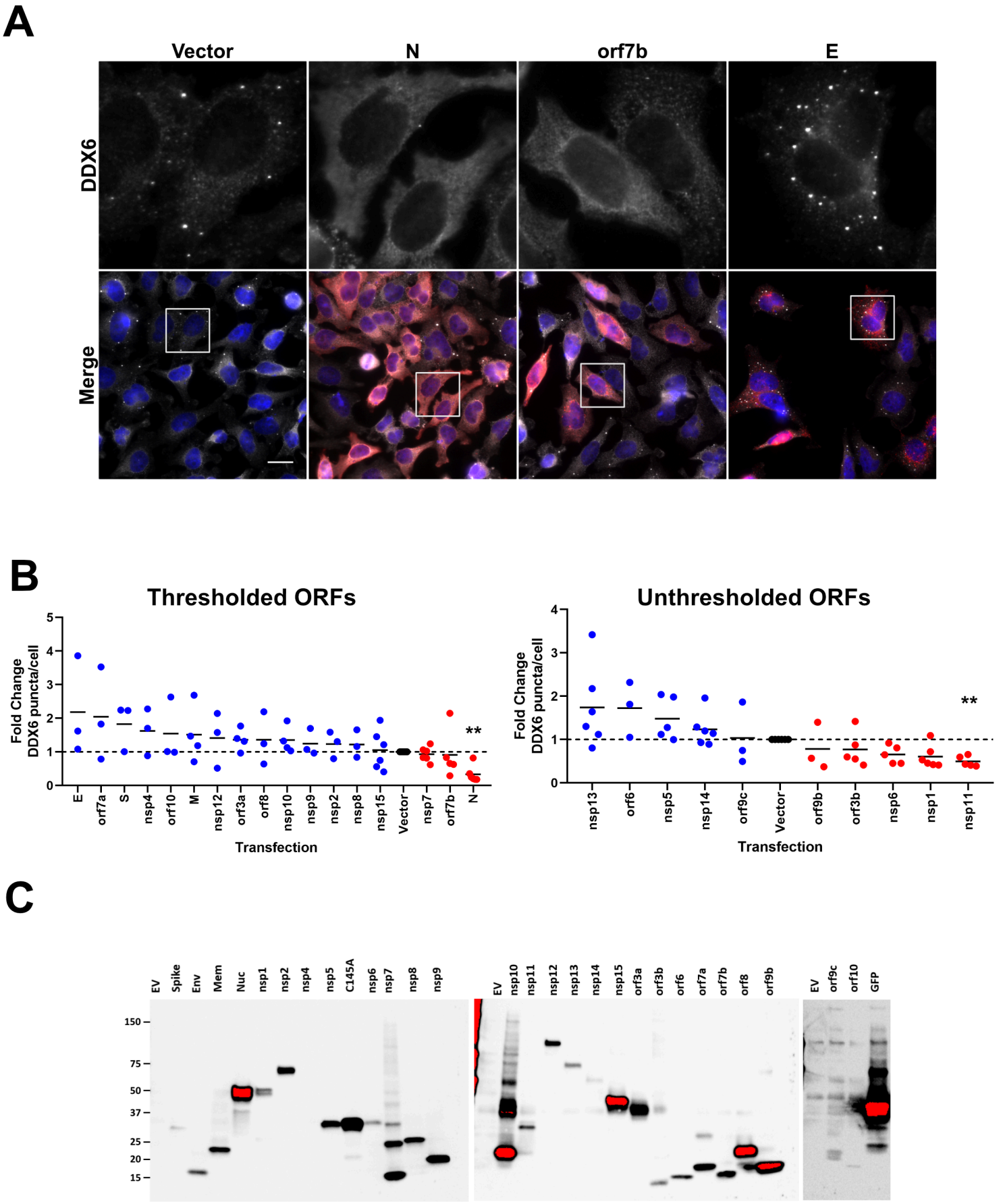
A
Vector
N
orf7b
E
DDX6
Merge
B
Thresholded ORFs
Fold Change DDX6 puncta/cell
Transfection
E
orf7a
S
nsp4
orf10
M
nsp12
orf3a
orf8
nsp10
nsp9
nsp2
nsp8
nsp15
Vector
nsp7
orf7b
N
**
Unthresholded ORFs
Fold Change DDX6 puncta/cell
Transfection
nsp13
orf6
nsp5
nsp14
orf9c
Vector
orf9b
orf3b
nsp6
nsp1
nsp11
**
C
EV
Spike
Env
Mem
Nuc
nsp1
nsp2
nsp4
nsp5
C145A
nsp6
nsp7
nsp8
nsp9
150
75
50
37
25
20
15
EV
nsp10
nsp11
nsp12
nsp13
nsp14
nsp15
orf3a
orf3b
orf6
orf7a
orf7b
orf8
orf9b
EV
orf9c
orf10
GFP

A

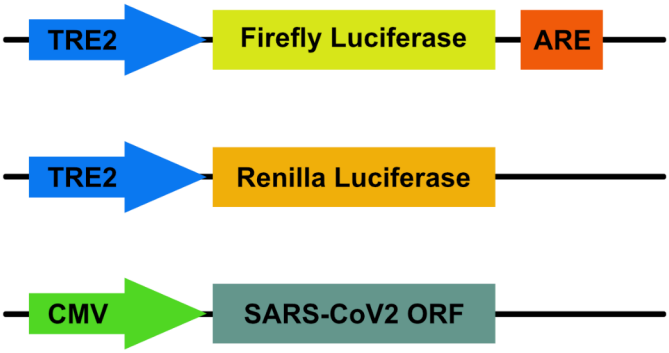
TRE2
Firefly Luciferase
ARE
TRE2
Renilla Luciferase
CMV
SARS-CoV2 ORF

B

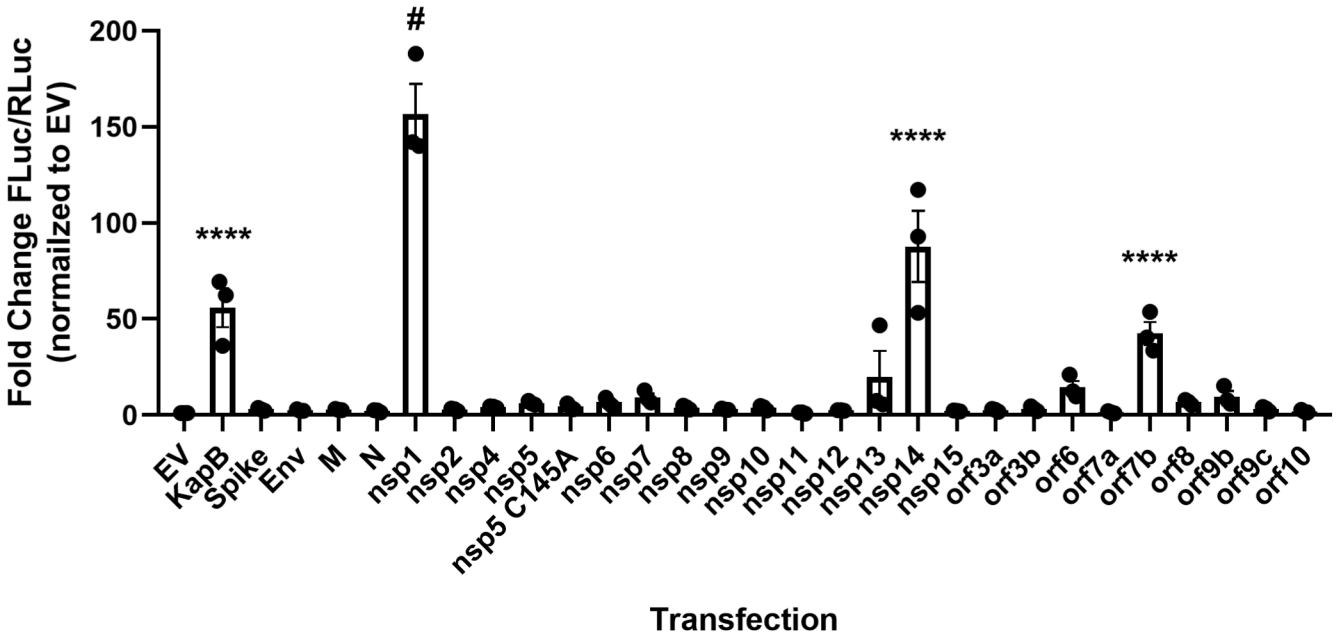
Fold Change FLuc/RLuc
(normailzed to EV)
200
150
100
50
0
#
****
****
****
EV
KapB
Spike
Env
M
N
nsp1
nsp2
nsp4
nsp5
nsp5 C145A
nsp6
nsp7
nsp8
nsp9
nsp10
nsp11
nsp12
nsp13
nsp14
nsp15
orf3a
orf3b
orf6
orf7a
orf7b
orf8
orf9b
orf9c
orf10
Transfection

A

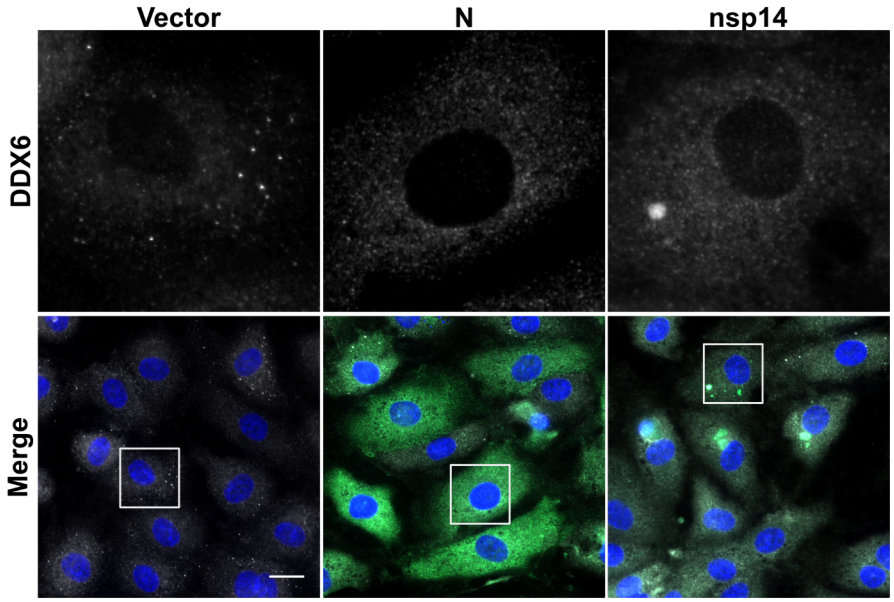
Vector
N
nsp14
DDX6
Merge

B

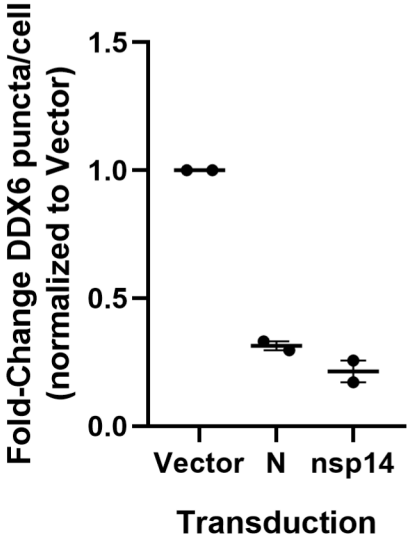
Fold-Change DDX6 puncta/cell
(normalized to Vector)
1.5
1.0
0.5
0.0
Vector
N
nsp14
Transduction

C

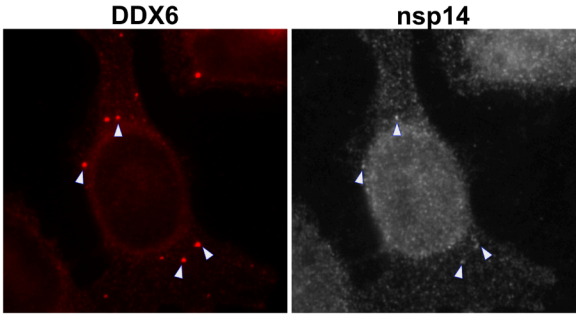
DDX6
nsp14

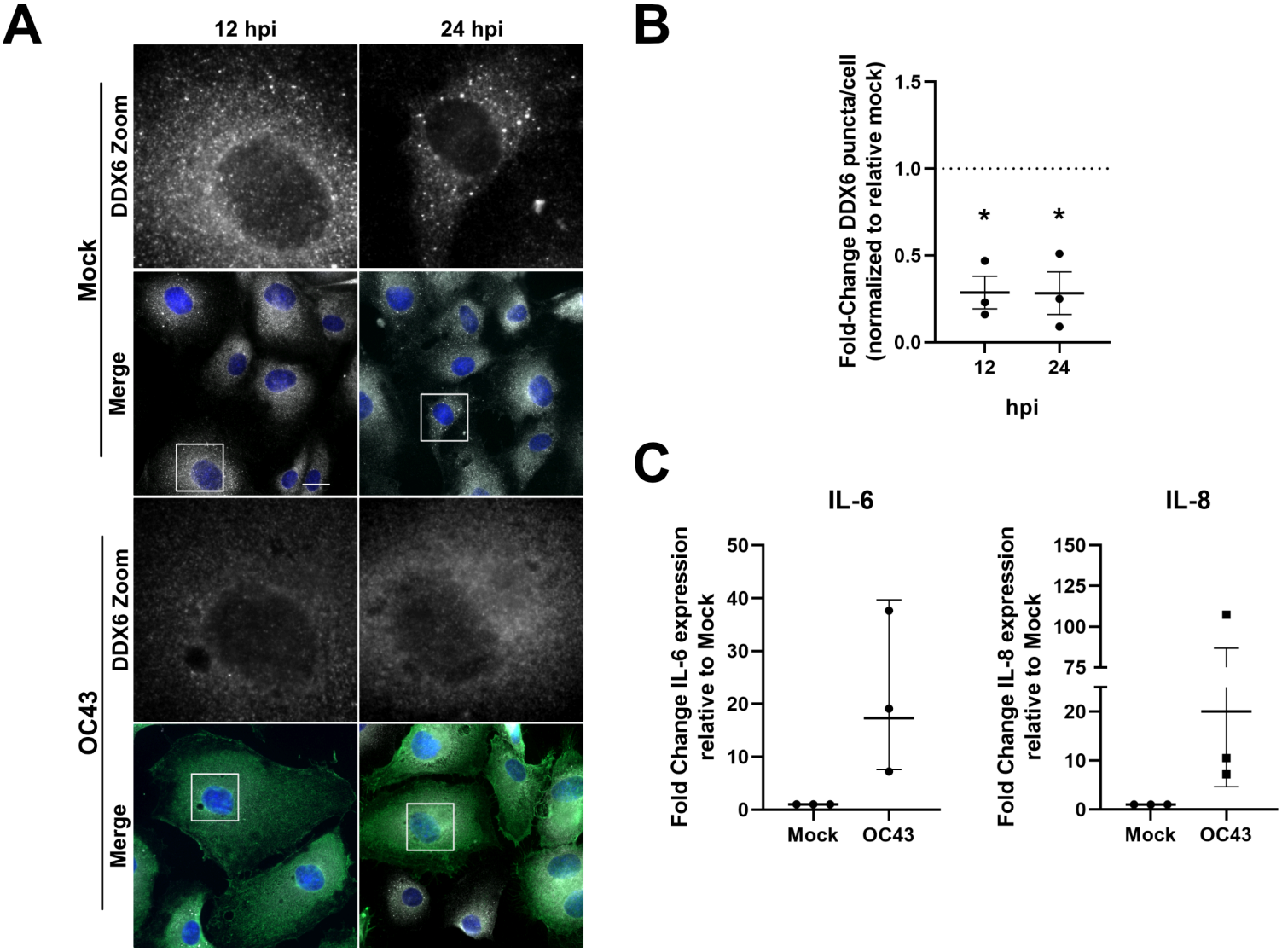
A
12 hpi
24 hpi
Mock
DDX6 Zoom
Merge
OC43
DDX6 Zoom
Merge
B
Fold-Change DDX6 puncta/cell (normalized to relative mock)
1.5
1.0
0.5
0.0
*
*
12
24
hpi
C
IL-6
Fold Change IL-6 expression relative to Mock
50
40
30
20
10
0
Mock
OC43
IL-8
Fold Change IL-8 expression relative to Mock
150
125
100
75
20
10
0
Mock
OC43

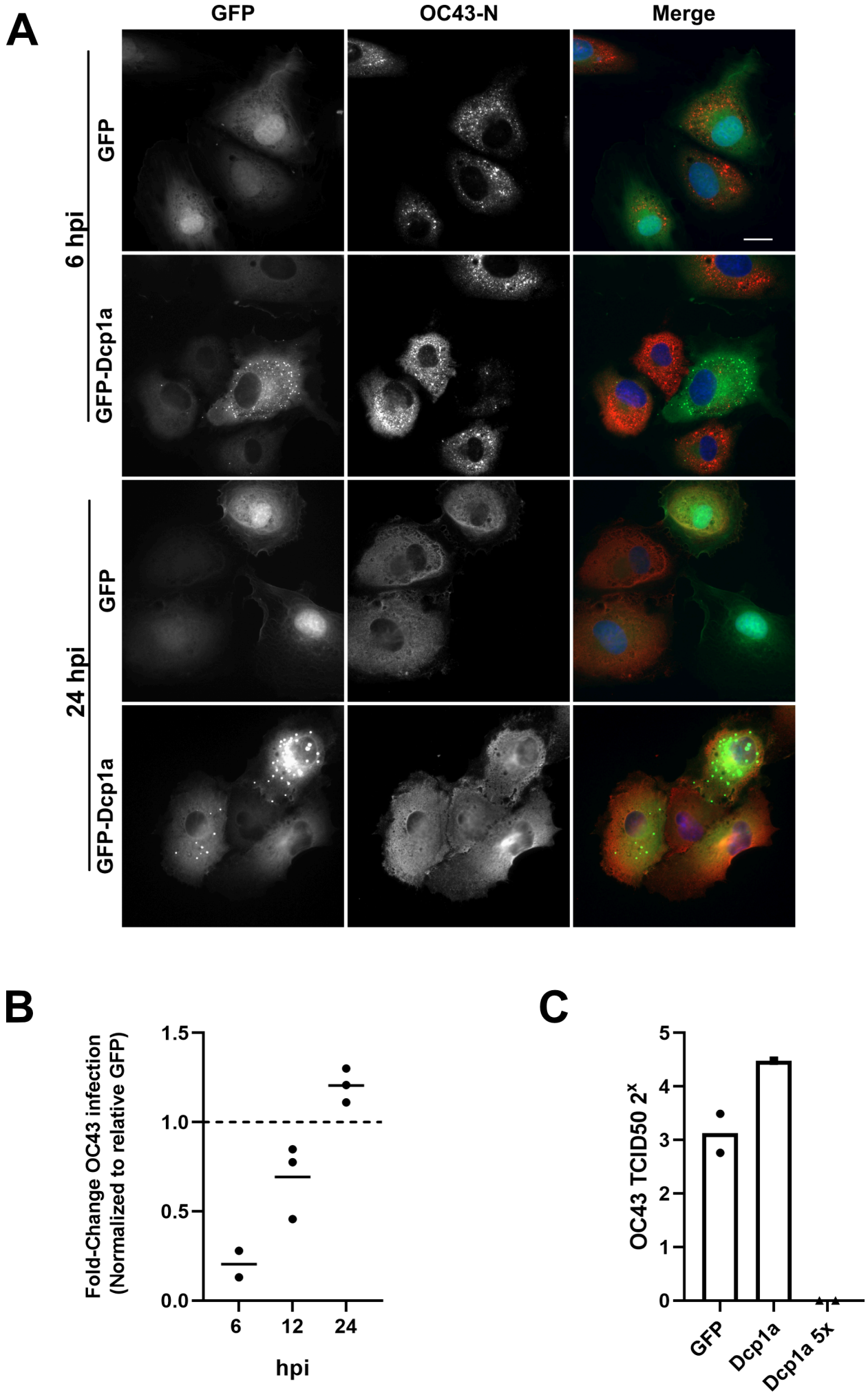
A
GFP
OC43-N
Merge
6 hpi
GFP
GFP-Dcp1a
24 hpi
GFP
GFP-Dcp1a
B
Fold-Change OC43 infection
(Normalized to relative GFP)
1.5
1.0
0.5
0.0
6
12
24
hpi
C
OC43 TCID50 2^x
5
4
3
2
1
0
GFP
Dcp1a
Dcp1a 5x

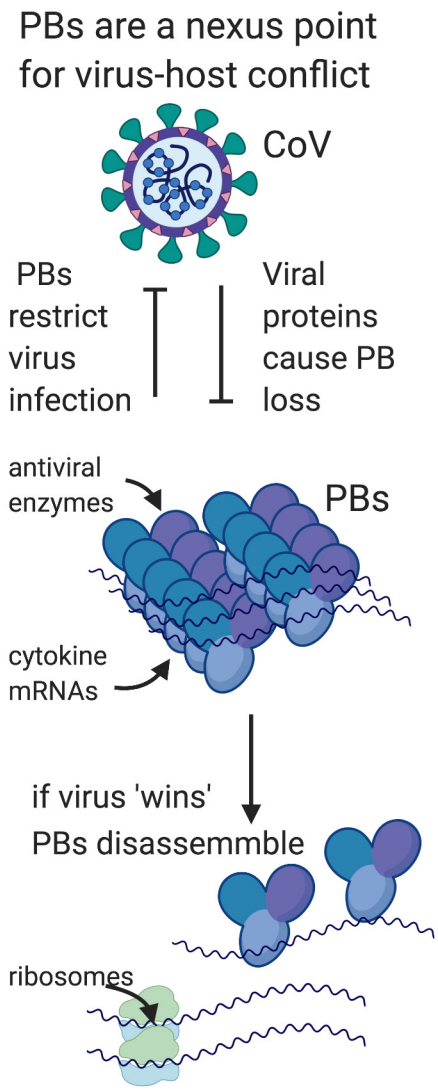

Repression of cytokine mRNA is relieved. This is an infected cell's call for reinforcements.

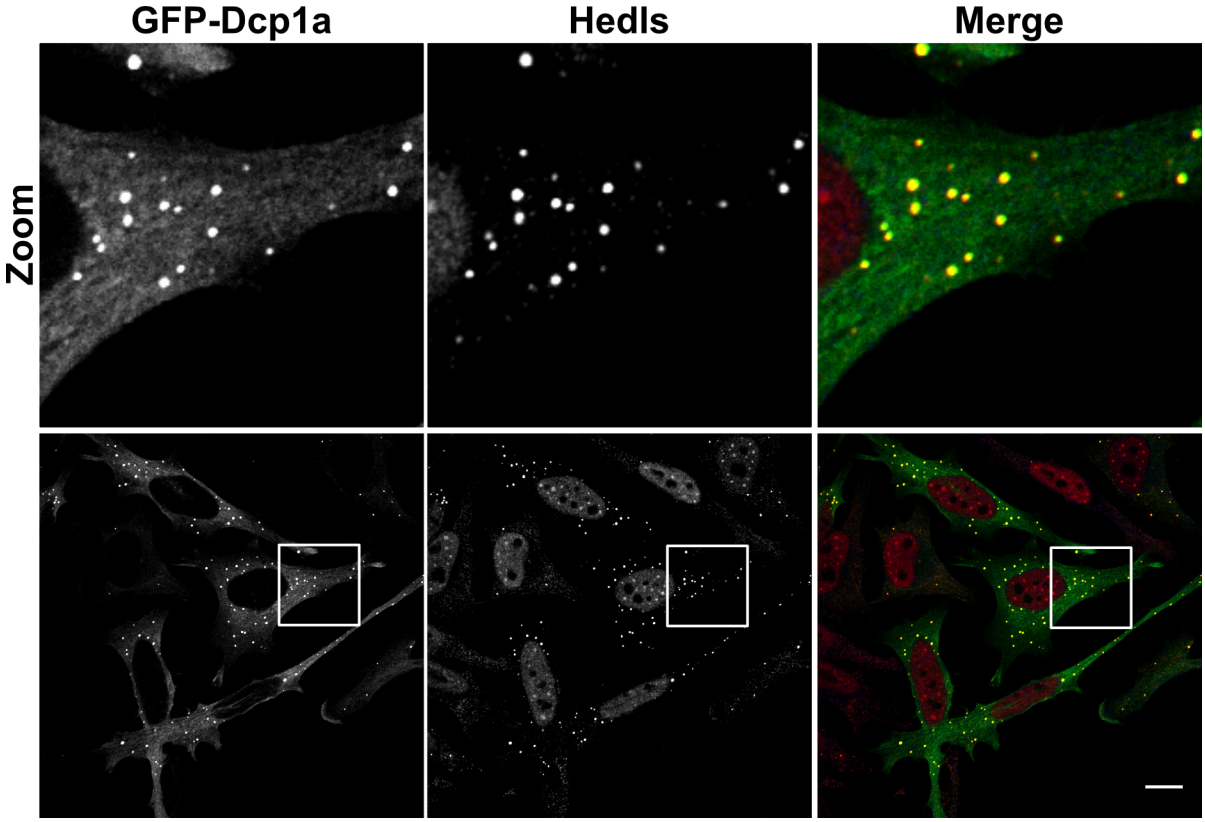
GFP-Dcp1a
Hedls
Merge
Zoom